Proceedings of the Liquid Metal Processing & Casting Conference 2019
Edited by: Alain Jardy, Alec Mitchell, and R. Mark Ward

MODELLING THE COLD CRUCIBLE POURING DYNAMICS

V. Bojarevics[1] and K. Pericleous[1]

[1] University of Greenwich, London SE10 9LS, UK

Keywords: titanium alloys, cold crucible, electromagnetic mixing, melting, particle tracking.

Abstract

The paper uses the mathematical modelling technique to investigate cold crucible operation with a non-consumable nozzle made of copper segments. The combination of two coils, one for the main crucible and the other for the nozzle with different power supplies, requires to superpose the effects of the two independent AC electromagnetic force fields. This leads to complex transitional flow structures and turbulence of the melt, contributing to the melt shape dynamics and the heat loss to the walls to satisfy the narrow balance between the thin solidified protective layer while avoiding the blockage of the outflow if the nozzle is frozen. The sensitivity of the outflow to the nozzle diameter is investigated. The beneficial features of the cold crucible melting to purify the melt from particulate contamination are explained using the particle tracking during the pouring process.

Introduction

Titanium alloys are increasingly used in aerospace and automotive applications. New melting techniques and practices are required to achieve desirable mechanical properties for critical components [1]. The cold crucible technique, alternatively known as the induction skull melting (ISM), is commonly used to melt the titanium alloys with additional stirring created by electromagnetic forces. The intense stirring is essential in preparing homogeneous alloys when adding uniformly dispersed grain refiners or micro- to nano- size particles to create a composite alloy of enhanced mechanical properties [2]. At the same time refinement of the alloy from larger oxide particles and film fragments of macro size (100 micron and larger) is highly desirable. The ISM technique is proven to be most effective to obtain reactive metal castings and produce high quality metal powders. A critical step in casting these components is the way how the prepared liquid alloy is delivered to the casting mold. Using the tilt casting technique the liquid alloy experiences significant loss of the required superheat [6], therefore various bottom pouring techniques were proposed. The graphite/ceramics nozzle [1] is the most successful in industrial applications, however suffers from deterioration due to erosion and needs replacement after each casting. A new type of nozzle composed of copper segments was tried and tested in [4,5], however the design did not find a widespread application due to uncontrollable outflow from the crucible and the low energy efficiency. Therefore a new type of copper nozzle is proposed in this paper. This nozzle is intended to replace the existing ceramics nozzle by a suitable size copper nozzle composed of water cooled segments. To design this nozzle a careful selection of the operating parameters is required accounting for the solidifying skull formation and the melt outflow to the nozzle.

There is a variety of mathematical modelling attempts of the ISM to mention just the few representative publications [3-7] and the references therein. The present paper presents the fully dynamic simulation of the melting including the dynamic free surface resolution during the full

bottom pouring cycle of the cold crucible operation. This is achieved using the previously validated spectral code SPHINX [6,7].
The code is supplemented by the Lagrangian particle tracking module in attempts to give insight to the behavior of various inclusions and possible separation in the ISM process [7]. The large scale electromagnetically driven flow circulation exerts a drag force which contributes to the particle transport [7]. The particles travel due to the hydrodynamic drag, buoyancy, turbulent fluctuations and the electromagnetic force action via the local pressure distribution around the particle. A significant contribution to the force balance arises from the so called electro-magnetophoretic forces [8], which are well known for a variety of MHD applications, such as removal of inclusions from steel melt [9], concentrating electrically insulating bubbles or particles towards the surface [10], and for many other purposes of separation or mixing [7]. The electromagnetic force acts directly onto electrically conducting inclusions, however the electromagnetic force in the surrounding fluid creates the pressure distribution gradient leading to the integral force on the non-conducting inclusions as well. Experimental observations of the particles of various shapes and electrical conductivities in the liquid metal carrying electrical current are described in [11], where the expression similar to Leenov, Kolin's [8] was derived, but for the conditions of gradient magnetic field, which results in the increase of the effective force on the particles. In the AC magnetic field the time average force effects are often treated using the same formulae as for the constant uniform fields [7-10]. The latter contradicts the skin-layer distribution of the AC field magnitude exponentially rising near the metal surface. Moreover, the total force in AC field contains also the pulsating part contributing to the particle drag by the 'history' and 'added mass' contributions [12,13]. The high mixing rates ensure the intense turbulence in the bulk of molten metal, which additionally affects the particle dispersion due to the turbulent velocity pulsations.
The paper demonstrates the importance of the AC magnetic interaction effects on the particle transport and the eventual separation during the cold crucible operation accounting for the solidifying skull formation and the melt outflow to the nozzle at the bottom. The non-consumable nozzle made of copper segments could help to solve the problem of the short life cycle of traditional graphite/ceramics type of nozzles used in the existing ISM devices [1].

Mathematical Model

The equations solved by the numerical model are the momentum and mass conservation equations for the incompressible fluid with the effective viscosity ν_e and the turbulent diffusivity α_e modified heat transfer equations:

$$\partial_t \mathbf{v} + (\mathbf{v}\cdot\nabla)\mathbf{v} = -\rho^{-1}\nabla p + \nabla\cdot(\nu_e(\nabla\mathbf{v} + \nabla\mathbf{v}^T)) + \rho^{-1}\mathbf{f}_{AC} + \mathbf{g}\,, \tag{1}$$

$$\nabla\cdot\mathbf{v} = 0\,, \tag{2}$$

$$C_p^*(\partial_t T + \mathbf{v}\cdot\nabla T) = \nabla\cdot(C_p\alpha_e\nabla T) + \rho^{-1}\,|\,\mathbf{J}\,|^2/\sigma\,, \tag{3}$$

The usual notation is used, given in detail elsewhere [7]. The full boundary conditions for the velocity include the no-slip condition at the solid container walls

$$\mathbf{v} = 0\,, \tag{4}$$

at the free surface the normal stress is determined by the pressure p_a in the space above the crucible and the surface tension:

$$\mathbf{e_n} \cdot \Pi \cdot \mathbf{e_n} = p_a + \Gamma K . \tag{5}$$

The pressure p_b is prescribed at the nozzle exit. On the liquid metal free surface the continuity of the velocity field and the tangential stress conditions are required:

$$\nabla \cdot \mathbf{v} = 0, \quad \mathbf{e_n} \cdot \Pi \cdot \mathbf{e}_\tau = 0, \tag{6}$$

where $\boldsymbol{e_n}, \boldsymbol{e}_\tau$ are the unit vectors normal and tangential to the free surface, Π is the stress tensor, K is the surface curvature. The free surface shape **R**(t) is updated at each time step using the kinematic condition:

$$\partial_t \mathbf{R} \cdot \mathbf{e_n} = \mathbf{v} \cdot \mathbf{e_n} \tag{7}$$

The previously validated [6] 'k-ω' turbulence model including the effect of magnetic damping is used to calculate the effective viscosity ν_e and the turbulent diffusivity α_e. The thermal boundary conditions account for the radiation losses, the high vapour pressure alloy component evaporation, and the heat loss to the water-cooled solid surface of the crucible and the nozzle [6].

In the pseudo-spectral code SPHINX the electromagnetic force is computed from an integral equation representation. This has an advantage that the boundary conditions are not explicitly required and the electromagnetic field can be solved only in the regions where it is needed. The electric current distribution in a moving medium of conductivity σ is then given by the magnetic vector potential **A**, the magnetic field $\mathbf{B} = \nabla \times \mathbf{A}$, the electric potential φ and the fluid flow induced part $\sigma \mathbf{v} \times \mathbf{B}$:

$$\mathbf{j} = \sigma(-\partial_t \mathbf{A} - \nabla\varphi + \mathbf{v} \times \mathbf{B}) = \mathbf{j}_{AC} + \mathbf{j}_v . \tag{8}$$

The $\mathbf{j}_{AC}$ part of the current is induced in the conducting medium even in the absence of velocity. The governing integral equations can be obtained from the electric current distribution in the source coils and the unknown induced currents in the liquid related to the total magnetic field and the vector potential **A** by the Biot-Savart law:

$$\mathbf{A}(\mathbf{r}) = \tfrac{1}{4\pi} \int \mathbf{j}(\mathbf{r}')/|\mathbf{r} - \mathbf{r}'| \, \mathrm{d}\mathbf{r}' \tag{9}$$

The equations (8) and (9) can be solved efficiently in the axisymmetric case for harmonic fields. The induced current in the liquid drop depends on its instantaneous free surface shape and needs to be recomputed as the shape changes during the oscillation development. The resulting electromagnetic force **f**, time-averaged over the AC period, similarly to (8) can be decomposed in two parts: $\mathbf{f} = \mathbf{f}_{AC} + \mathbf{f}_v$. The second, fluid velocity dependent part of the force $\mathbf{f}_v$ can include DC and AC time-averaged contributions. In the presence of AC fields originating from different sources, as in the ISM containing the main coil at the side of the crucible and the bottom coil at the nozzle, the superposition of the time average force contributions and the Joule heating in the liquid metal are used.

The equations (1)-(9) are solved by the spectral collocation method with the Chebyshev grid for the radial direction and Legendre nodes in the vertical direction. The numerical solution method is based on the continuous co-ordinate transformation adapting to the free surface and the containing vessel shape at the consecutive time steps. The stable time integration of the solution is based on adjustable time steps of the order 0.1 – 2 ms for the unsteady fluid flow solution in the examples considered below.

Particle Tracking

The present code implementation includes the Lagrangian passive particle tracking algorithm. The position **R**(x,y,z,t) of a large number (N~1000) of individual particles can be determined following their paths and the variable total force **F**(x,y,z,t) acting on each of the particles by solving the set of two equations [10]:

$$\partial_t \mathbf{R} = \mathbf{u}_p, \quad m_p \partial_t \mathbf{u}_p = \mathbf{F}, \tag{10}$$

where $\mathbf{u}_p$ is the particle velocity and m_p its mass. The force **F** acting locally on the spherical particle can be decomposed into the instantaneous fluid drag force $\mathbf{F}_d$ (depending on the local Reynolds number Re_p), the memory Basset force, the added mass force (see [11]), the buoyancy force $\mathbf{F}_g$ and the effective electromagnetic force $\mathbf{F}_e$. The electromagnetic force acts on the electric current penetrating the particle and additionally due to the fluid pressure redistribution on the surface of the particle [11]. For the case of electrically non-conducting particles (oxides, carbides, dendrite fragments, bubbles etc.) the effective electromagnetic force action in the AC skin-layer can be derived as $\mathbf{F}_e = -V_p(\frac{3}{2}\widehat{\mathbf{f}}_e + \mathbf{f}'(t))$, the sum of the time average and the oscillating components in the fluid at the location of the particle. Note, the Leenov, Kolin [8] expression derived for the DC only constant fields gives two times smaller force acting on a non-conducting particle.

The typical mixing flow in the cold crucible is turbulent ($Re \sim 10^3$ - 10^4), which requires a modification for the $\mathbf{F}_d$ calculation due to the stochastic part of velocity in accordance to the resolved turbulent kinetic energy k and the local eddy life time (or the particle transit time in that eddy, whichever is the shortest). The use of k- ω turbulence model in the SPHINX code facilitates to obtain these quantities, which are locally interpolated to the particle position at each time step. The numerical integration of equations (1) and (2) is done for each individual particle of various properties depending on the initial seeding locations. The exponential numerical scheme permits the stable time integration of the particle tracks using adjustable time steps of the order 0.1 - 1ms used for the unsteady fluid flow solution in the examples considered below.

Simulation Results

The mathematical modelling of the complex time dependent problem starts initially with heating a cylindrical TiAl solid of 50 kg weight, leading to the gradual melting process and subsequent liquid metal magnetic confinement dynamics, turbulent fluid flow and the temperature evolution. In the present ISM setup two different coils are used: one at the side (lower frequency ~ 5 kHz) and the second smaller at the nozzle (~50 kHz). The time dependent Joule heating eventually leads to melting of the solid ingot. When the solidus temperature is reached, the model accounts for the phase transition and the following liquid material shape change due to the action of the EM force distribution adjusted to the moving solid/liquid and the free interface. The electromagnetic field induces a strong turbulent flow in the molten pool, which is beneficial for producing a

homogeneous melt with uniform temperature. The process combines induction melting and pouring via the bottom nozzle into a single self-controlling operation.

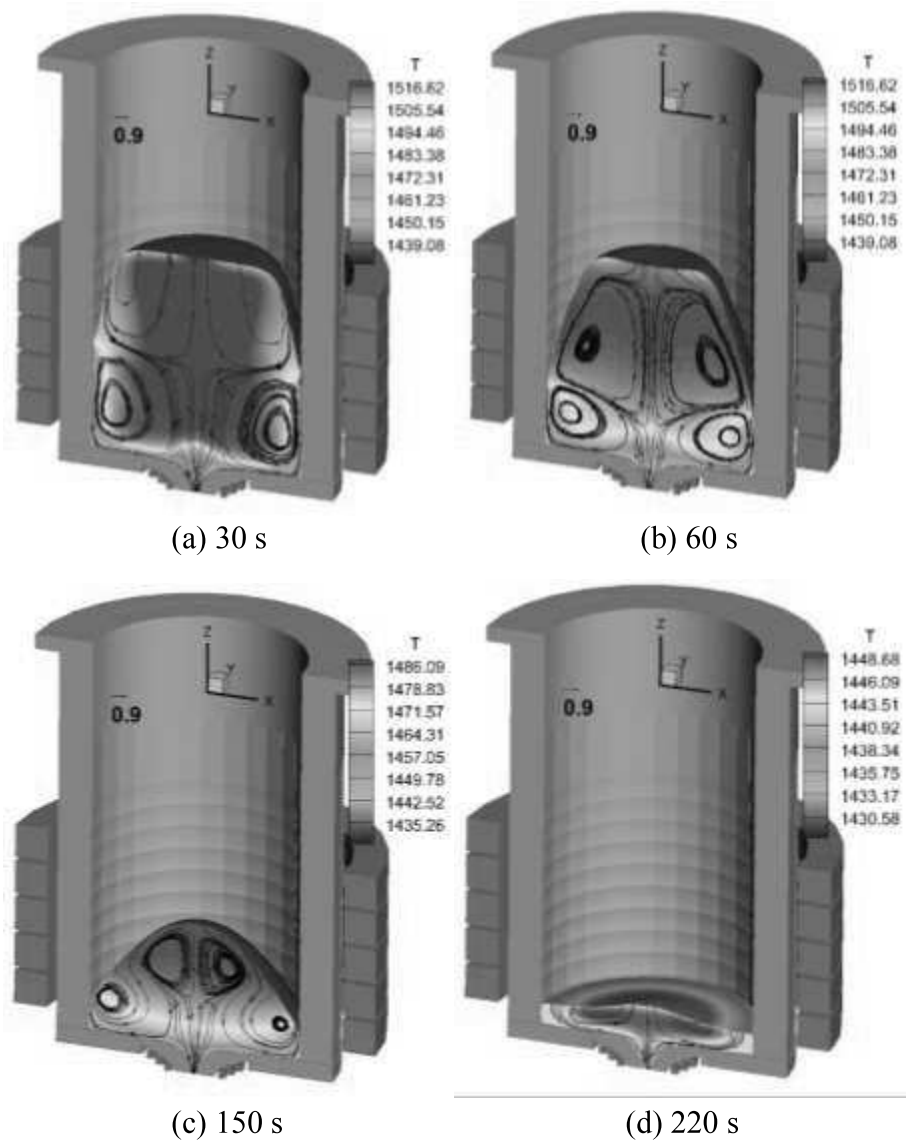

Figure 1. Dynamic stages of the cold crucible operation with the nozzle d = 8 mm: a) the initial stage after complete melting is achieved, b) the following stage when pouring starts, the volume decreases and the dome shape is stabilised, c) the late stage of pouring when the power coupling is reduced, d) the final stage just before the end of pouring.

After the initial melting stage practically all volume of the titanium aluminide alloy is in liquid phase shaped as typical dome (Figure 1a). The action of the bottom coil at all following stages (Figure 1) helps to maintain the nozzle free from solid phase, except from the extremely thin solidified skull acting as a protecting film between the out flowing liquid metal and the copper segmented wall of the nozzle. The side skull thickness gradually grows, particularly in the bottom part, until the accelerated solidification starts at the end stages of the pouring (Figure 1d) due to

the fast decrease of inductive coupling to the melt and decrease in the Joule heating delivered to the melt (Figure 2).

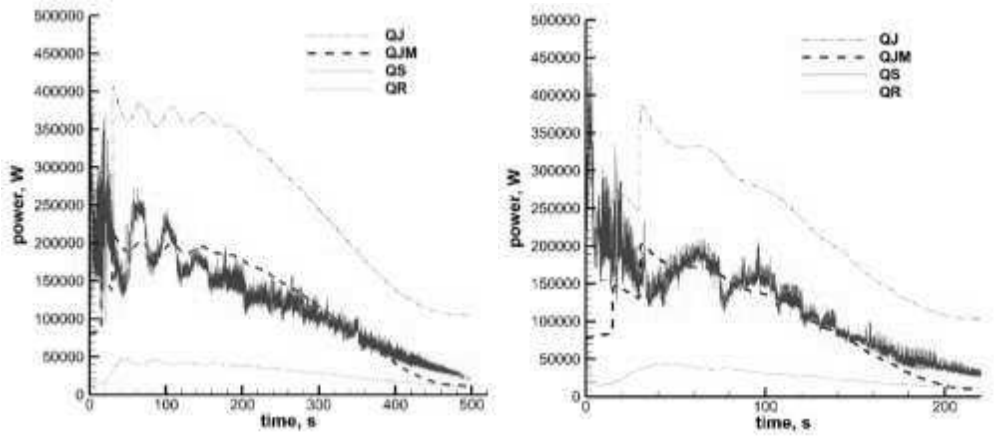

(a) 6 mm (b) 8 mm

Figure 2. The time dependent variation of the induced electric heating and losses: (a) for the nozzle opening of 6 mm and (b) for 8 mm opening. QJ is the total Joule heating of the melt and the copper walls, QJM – melt only, QS – losses to the wall by the turbulent heat transfer, QR – radiation losses from the free surface.

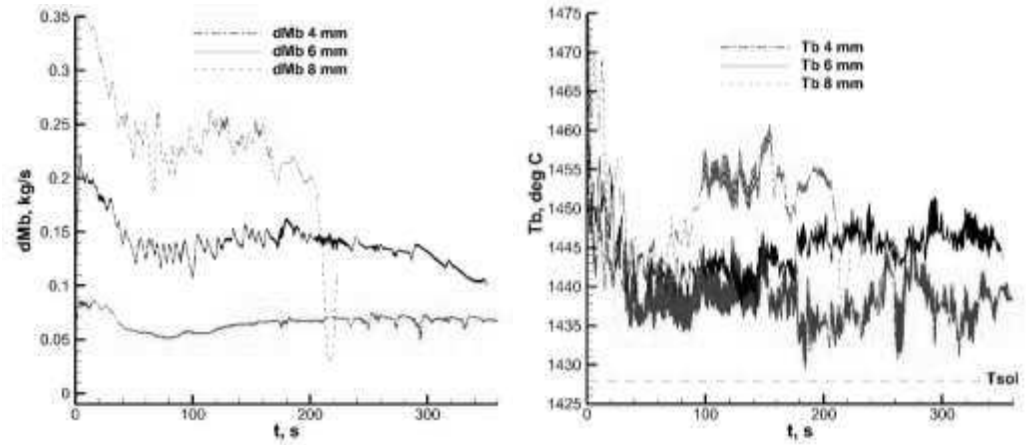

(a) pouring rate (b) temperature at exit

Figure 3. The liquid metal pouring rate in kg/s and the temperature in C^o at the exit nozzle for the nozzle opening diameters 4, 6 and 8 mm.

The action of the EM force in the nozzle region affects the outflow rate which is monitored during the full simulation cycle. The Figure 3 shows the predicted outflow rate and the moderate superheat of about 20 degrees C, which is fluctuating due to the turbulent flow and the free metal surface oscillation. The average temperature drops with the decrease in the Joule heating delivered to the melt. The outflow rate depends significantly on the nozzle diameter as shown in the Figure 3. The

outflow rate and its stability can be controlled additionally by adjusting the current magnitude and the AC frequency of the nozzle surrounding coil. This is particularly important if a slow rate outflow is desired. The narrow nozzle of 4 mm diameter requires a careful adjustment of the current and frequency to prevent unstable outflow. The Figure 4 shows the final stages of the crucible operation when the bottom skull grows fast and the nozzle eventually freezes over. Even at this stage it is possible to remelt the frozen nozzle exit if increasing the current in the bottom coil, however the heat removal in the bottom copper segments need to be strictly controlled.

(a) 800 s (b) 870 s

Figure 4. The cold crucible operation with the nozzle d = 4 mm: a) the late stage of pouring when the power coupling is reduced, b) the final stage just before the end of pouring when the nozzle freezes over.

Particle Tracking Results

The impurity particle distribution were simulated by adding the aluminium oxide particles on the surface of the liquid metal at the fully molten stage. 3*300 particles of three sizes (1, 20 and 50 μm) were dynamically followed during the full pouring cycle in order to follow their tracks, extraction or separation routes. There is a remarkable difference in the particle behavior depending on EM force effect on particles. The sequence of the particle distribution can be compared from the Figures 5 and 6. The largest particles of 50 μm size are completely separated to the solid side skull region and remain there in spite of the vigorous mixing in the melt when the EM effects are accounted computing the time dependent forces during the particle propagation in the melt. A limited amount of the smaller particles (1 and 20 μm) eventually pass to the nozzle exit, while the majority are captured in the bottom and side solidified skull (Figure 5). This behavior is in sharp contrast to the particle distribution computed in exactly the same way, except excluding the effective electromagnetic force $\mathbf{F}_e$ action on the particles in the equation (2).

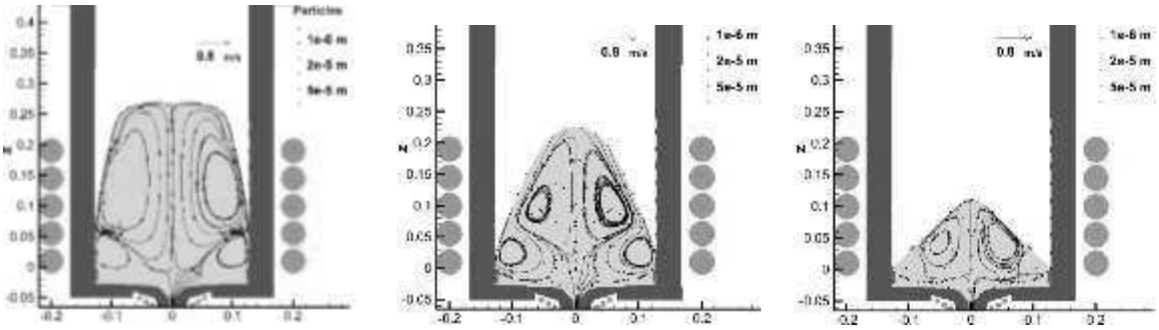

a) b) c)

Figure 5. Dynamic stages of the particle tracking *with the EM pressure effect* on the particles: a) the initial stage after complete melting, particles introduced on the surface are retained from spreading into the melt, b) only the small size 1-20 μm particles are partially dispersed, c) at the late stage of pouring large particles are extracted to the 'skull' and a limited number of small particles travel to the nozzle.

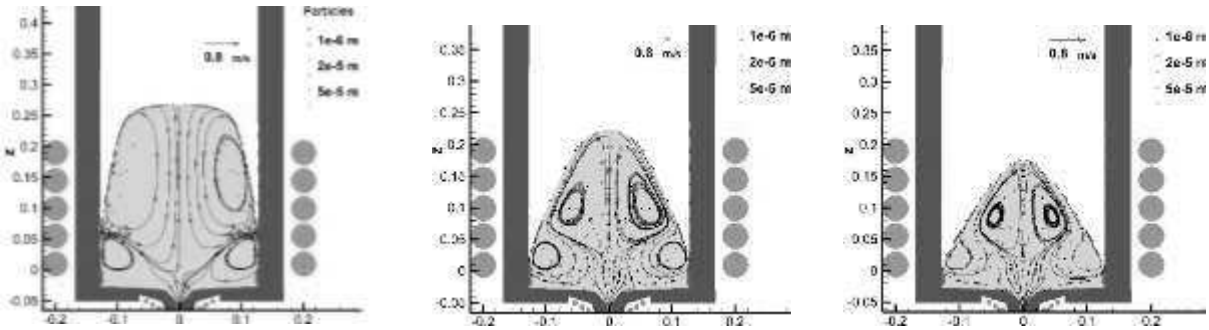

a) b) c)

Figure 6. Dynamic stages of the particle tracking *without the EM effect* on the particles: a) the initial stage after complete melting, particles introduced on the surface start spreading into the melt, b) the particles are dispersed at mid-stage of the pouring, c) at the late stage of pouring all sizes of particles travel through the nozzle.

Conclusions

The beneficial features of the cold crucible melting to purify the melt are explained using the numerical modelling with the dynamic particle tracking. The non-consumable nozzle design is presented in principle, however leaving the specific parameters open to optimization and further discussion.

References

1. R.E. Haun, "Advances in the Systems and Processes for the Production of Gamma Titanium Aluminide Bars and Powder''. *JOM*, 69, N 12 (2017), 2615-2620.

2. W.H. Sillekens, et al. “The ExoMet Project: EU/ESA Research on High-Performance Light-Metal Alloys and Nanocomposites,’’ *Metall.Materials Trans*., 45A (2014), 3349–3361.
3. H. Tadano, M. Fujita, T. Take, K. Nagamatsu, A. Fukuzawa, “Levitational Melting of Several Kilograms of Metal with a Cold Crucible,’’ *IEEE Trans. Magn*., 30(6) (1994), 4740-4742.
4. T. Okumura, T. Shibata, N. Okochi, “Production of Ti Alloy Gas Atomized Powder by Levitation Melting Furnace with Electric Nozzle,’’ *Proc. 5th Internat. Conf. Electromagnetic Processing Materials*, Sendai, Japan, (2006), 784-789.
5. T. Okumura, K. Yamamoto, M. Shibata,. Large Scale Cold Crucible Levitation Melting Furnace with Bottom Tapping Nozzle,’’ *Proc. 6th Internat. Conf. Electromagnetic Processing Materials*, Dresden, Germany, (2009), 521-524.
6. V. Bojarevics, R.A. Harding, K. Pericleous and M. Wickins The Development and Experimental Validation of a Numerical Model of an Induction Skull Melting Furnace *Metall. Materials Trans.*, 35B (2004), 785-803.
7. V. Bojarevics, K. Pericleous, Electromagnetic particle separation in the cold crucible melting with novel type bottom pouring nozzle. *Proc. 9th Internat. Conf. Electromagnetic Processing Materials*, IOP Conf. Series: Materials Science and Engineering, 424, 012029 (2018). doi:10.1088/1757-899X/424/1/012029
8. D. Leenov and A. Kolin, *Journ. Chem. Phys.*, 22, N 4 (1954) 683-688.
9. V. Bojarevics, J. Freibergs, E. Shilova, E. Shcherbinin, Electrically Induced Vortical Flows, Kluwer Academic Publishers, Dordrecht, Boston, London, (1989).
10. R. Clift, J.R. Grace, M.E. Weber, Bubbles, Drops, and Particles, Dover Publications, Mineola, New York, (2005).
11. L.D. Landau and E.M. Lifshitz, Fluid Mechanics, Pergamon Press, (1987).